RAA 2021 Vol. **21** No. **5**, 109(13pp) doi: 10.1088/1674-4527/21/5/109

http://www.raa-journal.org *http://iopscience.iop.org/raa*

***R**esearch in*
***A**stronomy and*
***A**strophysics*

A new class of viable and exact solutions of EFEs with Karmarkar conditions: an application to cold star modeling

Neeraj Pant[1], Megandhren Govender[2] and Satyanarayana Gedela[3]

[1] Department of Mathematics, National Defence Academy, Khadakwasla, Pune-411023, India; *neeraj.pant@yahoo.com*
[2] Department of Mathematics, Faculty of Applied Sciences, Durban University of Technology, Durban, South Africa; *megandhreng@dut.ac.za*
[3] Department of Mathematics, SSJ Campus, Kumaun University, Almora-263601, India; *satya235@gmail.com*

Received 2020 August 23; accepted 2020 November 22

Abstract In this work we present a theoretical framework within Einstein's classical general relativity which models stellar compact objects such as PSR J1614–2230 and SAX J1808.4–3658. The Einstein field equations are solved by assuming that the interior of the compact object is described by a class I spacetime. The so-called Karmarkar condition arising from this requirement is integrated to reduce the gravitational behaviour to a single generating function. By appealing to physics we adopt a form for the gravitational potential which is sufficiently robust to accurately describe compact objects. Our model satisfies all the requirements for physically realistic stellar structures.

Key words: Compact star — anisotropy — embedding class — Einstein field equations — adiabatic index

1 INTRODUCTION

Since the publication of Einstein's general relativity in 1914, researchers were captivated by the search for exact solutions of the field equations. Over the past century a myriad of exact solutions was obtained which attempted to explain observations in cosmology and astrophysics. The gravitational field exterior to a static, spherically symmetric star was first obtained by Schwarzschild in 1916. This vacuum solution was followed by the interior Schwarzschild solution which describes the gravitational field of a uniform density sphere (Schwarzschild 1916a,b). Causality is one of the cornerstones of relativity which requires $0 < \frac{dp}{d\rho} < 1$ (Dev & Gleiser 2002, 2003). It is clear that causality is violated at each interior point of the Schwarzschild constant density sphere. This prompted researchers to consider more realistic matter configurations which included inhomogeneous density profiles, anisotropic pressures, electric charge, bulk viscosity and scalar fields. Generalization of the perfect fluid interior matter distribution to include anisotropic stresses has yielded interesting physical characteristics of such models. It was demonstrated that physical properties such as surface tension, compactness and surface redshift of these stars are sensitive to the anisotropy parameter (Sharma & Maharaj 2007; Bowers & Liang 1974; Maurya & Govender 2017; Pant et al. 2016). The impact of electric charge in compact objects has been widely studied within the context of stability and physical viability. It was shown that the presence of electric charge alters the Buchdahl limit required for stability of a self-gravitating, bounded matter distribution (Singh et al. 2016; Andreasson et al. 2012). Departure from spherical symmetry has also been pursued in the context of slowly rotating stars and in the description of gravitational waves (Herrera et al. 2005a,b). Various techniques ranging from ad-hoc assumptions, imposition of pressure isotropy, application of an equation of state (EoS), use of the condition of conformal flatness and Lie symmetry analysis, to name just a few, were relied on to solve the field equations (Manjonjo et al. 2018; Ivanov 2018). While these methods yield solutions, there is no guarantee that the ensuing models are physically viable. An extensive review of exact solutions of the Einstein field equations (EFEs) describing static objects indicates that a very small subset of these satisfy all the requirements for realistic stellar models (Stephani et al. 2003).

A natural question which arises in astrophysics is what happens when a star loses hydrostatic equilibrium and undergoes continued gravitational collapse? Oppenheimer and Snyder tackled this problem by considering a spherically symmetric dust cloud undergoing gravitational

collapse (Oppenheimer & Snyder 1939). Their model served as a catalyst in understanding end-states of gravitational collapse. The Cosmic Censorship Conjecture which ruled out the formation of naked singularities for collapsing matter configurations with reasonable initial states was shown to be violated under various assumptions (Guo & Joshi 2015; Ghosh & Maharaj 2015; Sherif et al. 2019). The study of black holes has moved into the observable realm making it a popular research topic (Event Horizon Telescope Collaboration et al. 2019). Black hole physics has evolved immensely from the simple Oppenheimer-Snyder dust model to include anisotropic pressures, electromagnetic field, cosmological constant as well as higher dimensions.

Vaidya (1951) presented an exact solution describing the exterior gravitational field of a radiating star. This solution is a unique case of the EFEs describing a spherically symmetric atmosphere composed of null radiation. The Vaidya solution made it possible to model dissipative collapse in which the collapsing core radiates energy to the exterior spacetime in the form of a radial heat flux or null radiation. There were several early attempts at modeling a radiating star with a Vaidya exterior. The problem was matching the interior and exterior spacetimes across the boundary of the star. The junction conditions required for the smooth matching of a spherically symmetric, shear-free line element to Vaidya's outgoing solution were provided by Santos (1985). It was demonstrated that for a radiating spherical body dissipating energy in the form of a radial heat flux, the pressure on the boundary is proportional to the magnitude of the heat flux. This condition ensures conservation of momentum across the boundary of the collapsing body. Since the publication of the Santos junction conditions, there has been an explosion of models describing dissipative collapse starting with simple solutions and thus rapidly developing into more sophisticated stellar models. Herrera et al. (1989); Chan et al. (1994); Di Prisco et al. (2007); Herrera & Martinez (1998); Di Prisco et al. (1997) have been instrumental in investigating the nature of collapse with dissipation within a general framework, thus giving researchers rich insights into these problems, especially with the inclusion of shear, inhomogeneity and anisotropy. The thermodynamics of radiating stars was developed by Govender and co-workers since the early 1990s. Relaxational effects due to heat dissipation and shear viscosity predict temperature and luminosity profiles which are significantly different from the Eckart theory of thermodynamics (Govender et al. 2010; Govender 2013; Govender & Govinder 2001). Recently, there has been a resurgence in seeking exact solutions to the EFEs describing static, compact objects by employing the concept of embedding. The Karmarkar condition, which needs to be satisfied if the spacetime has to be a class I embedding, has been widely used to generate various stellar models describing anisotropic spheres (Karmarkar 1948). These models have been confirmed to satisfy all the stringent stability and physical tests imposed by the behaviour of the thermodynamic and gravitational variables (Bhar 2019; TellOrtiz et al. 2019; Maurya et al. 2019a; Jasim et al. 2020; Sing et al. 2020; Gedela et al. 2020; Ivano 2020; Sarkar et al. 2020). Many of these solutions have been reconciled with observational data of compact objects including strange stars, pulsars and neutron stars (Gedela et al. 2018, 2019a,b; Upreti et al. 2020; Fuloria 2017; Pant et al. 2020). By utilising a quadratic equation of state together with the Karmarkar condition, a model for the strange star candidate SAX J1808.4–3658 was obtained. It was shown that this model agrees with observational characteristics of this star. Furthermore, a comparison of the quadratic EoS model with modified Bose-Einstein condensation EoS and linear EoS was carried out (Gedela et al. 2019c). The Karmarkar condition has also been utilised to model dissipative collapse ensuing from an initially static configuration losing hydrostatic equilibrium and starts to radiate energy to the exterior spacetime. The Karmarkar condition together with the junction condition which represents conservation of momentum across the collapsing boundary determines the temporal and gravitational evolution of the model (Naidu et al. 2018). Many of these models indicate their robustness under the scrutiny of physical viability. To this end, we employ the Karmarkar condition to seek a model which accurately describes two stellar compact objects, namely, PSR J1614–2230 and SAX J1808.4–3658.

This paper is structured as follows: In Section 2, we present the EFEs describing the interior spacetime of the stellar model. The Karmarkar and embedding class I conditions are introduced in Section 3. By adopting a parametric form for one of the metric potentials we generate a stellar model in Section 4. Matching of the interior and exterior spacetimes is accomplished in Section 5. The physical features of the model are discussed in Section 6. We investigate the stability of our model in Section 7. The paper concludes with a discussion and finding our main results in Section 8.

2 THE EINSTEIN FIELD EQUATIONS

A line element within a spherically symmetric anisotropic fluid matter distribution in Schwarzschild coordinates $(x^i) = (t, r, \theta, \phi)$ is delineated in the following form

$$ds^2 = e^{\nu(r)}dt^2 - e^{\lambda(r)}dr^2 - r^2(d\theta^2 + \sin^2\theta d\phi^2), \quad (1)$$

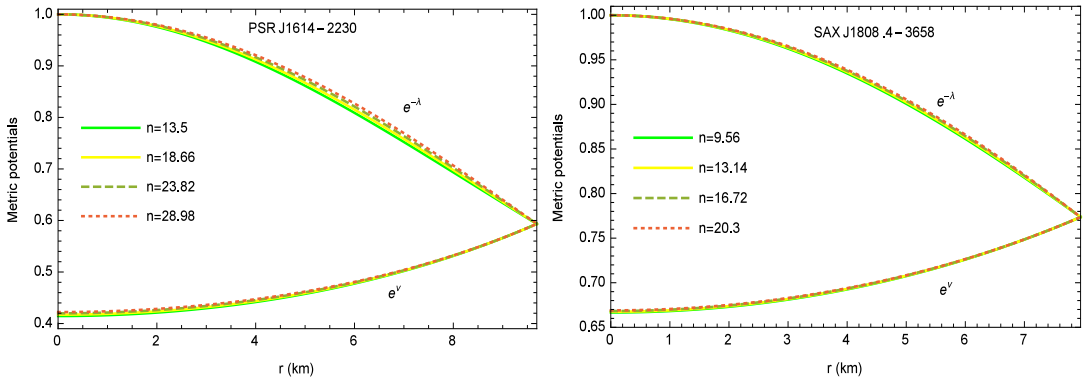

Fig. 1 Variation of $e^{-\lambda(r)}$ and $e^{\nu(r)}$ with r for (i) PSR J1614–2230 with mass $M = 1.97\,M_{\odot}$ and radius $R = 9.69$ km for the models $n = 13.5,\ 18.66,\ 23.82$ and 28.98; (ii) SAX J1808.4–3658 with mass $M = 0.9\,M_{\odot}$ and radius $R = 7.951$ km for the models $n = 9.56,\ 13.14,\ 16.72$ and 20.3, and the values $b = 0.0001\,\mathrm{km}^{-2}$ and $c = 2.5$.

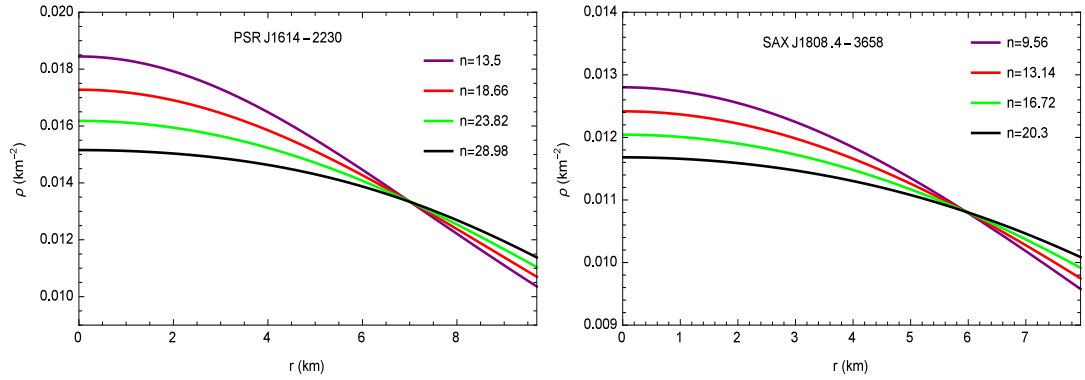

Fig. 2 Variation of ρ with r for (i) PSR J1614–2230 with mass $M = 1.97\,M_{\odot}$ and radius $R = 9.69$ km for the models $n = 13.5,\ 18.66,\ 23.82$ and 28.98; (ii) SAX J1808.4–3658 with mass $M = 0.9\,M_{\odot}$ and radius $R = 7.951$ km for the models $n = 9.56,\ 13.14,\ 16.72$ and 20.3, and the values $b = 0.0001\,\mathrm{km}^{-2}$ and $c = 2.5$.

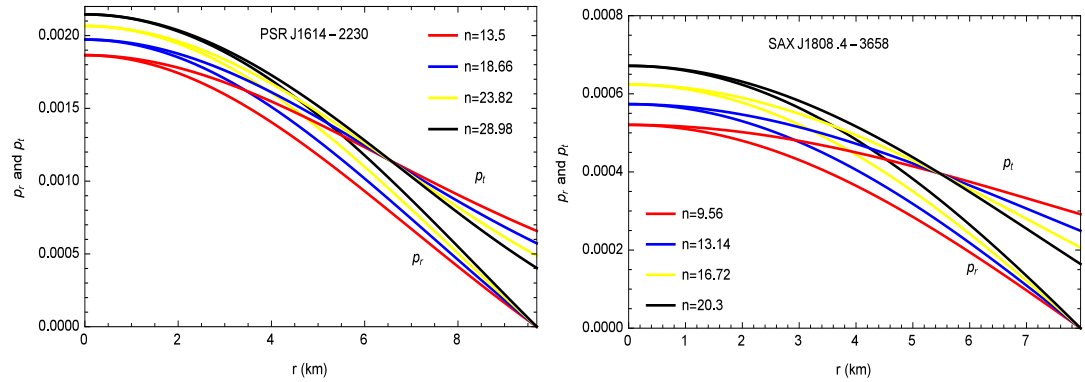

Fig. 3 Variation of p_r and p_t with r for (i) PSR J1614–2230 with mass $M = 1.97\,M_{\odot}$ and radius $R = 9.69$ km for the models $n = 13.5,\ 18.66,\ 23.82$ and 28.98; (ii) SAX J1808.4–3658 with mass $M = 0.9\,M_{\odot}$ and radius $R = 7.951$ km for the models $n = 9.56,\ 13.14,\ 16.72$ and 20.3, and the values $b = 0.0001\,\mathrm{km}^{-2}$ and $c = 2.5$.

where the gravitational potentials $\nu(r)$ and $\lambda(r)$ are yet unknown. The energy-momentum tensor for anisotropic matter takes the form

$$T_{jk} = [(p_t + \rho)v_j v_k - p_t g_{jk} + (p_r - p_t)\chi_j \chi_k], \quad (2)$$

where ρ, p_r and p_t are the energy density, and radial and transverse pressures respectively and p_t is in the perpendicular direction to p_r. The normalised 4-velocity vector $v^j = \sqrt{\frac{1}{g_{tt}}}\delta^j_t$ and the unit spacelike vector $\chi^j =$

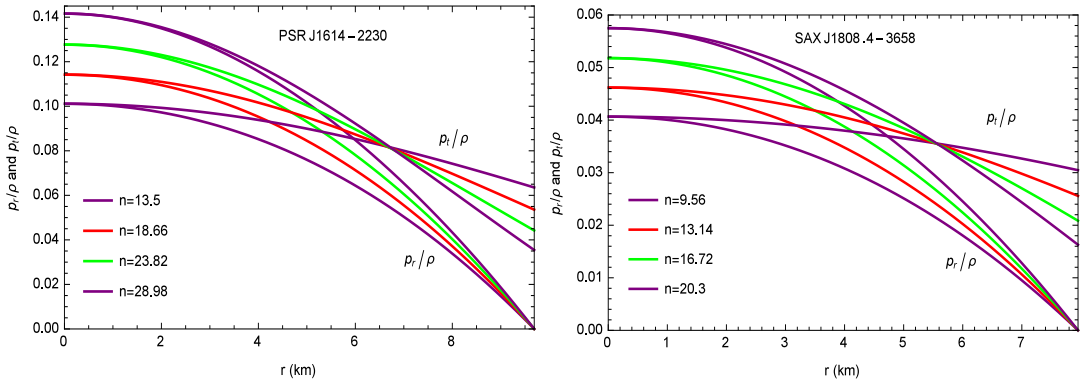

Fig. 4 Variation of p_r/ρ and p_t/ρ with r for (i) PSR J1614–2230 with mass $M = 1.97\,M_\odot$ and radius $R = 9.69$ km for the models $n = 13.5,\ 18.66,\ 23.82$ and 28.98; (ii) SAX J1808.4–3658 with mass $M = 0.9\,M_\odot$ and radius $R = 7.951$ km for the models $n = 9.56,\ 13.14,\ 16.72$ and 20.3, and the values $b = 0.0001\,\mathrm{km}^{-2}$ and $c = 2.5$.

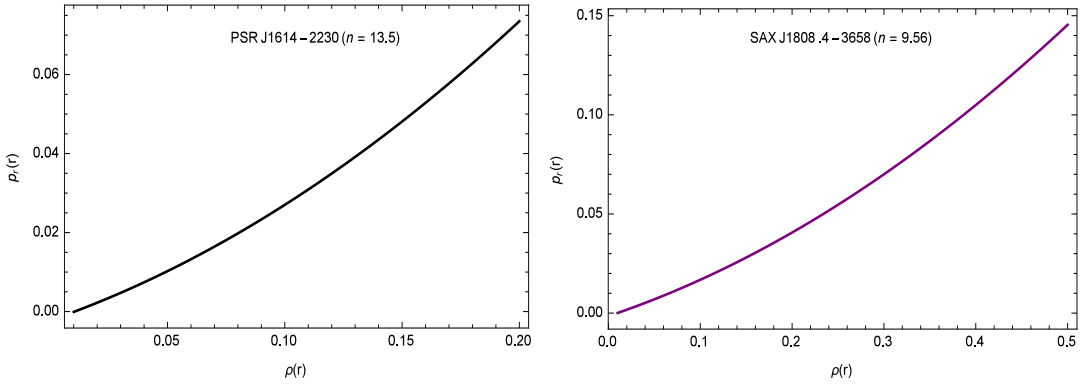

Fig. 5 Variation of EoS parameters with ρ for (i) PSR J1614–2230 with mass $M = 1.97\,M_\odot$ and radius $R = 9.69$ km for the model $n = 13.5$; (ii) SAX J1808.4–3658 with mass $M = 0.9\,M_\odot$ and radius $R = 7.951$ km for the model $n = 9.56$ and the values $b = 0.0001\,\mathrm{km}^{-2}$ and $c = 2.5$.

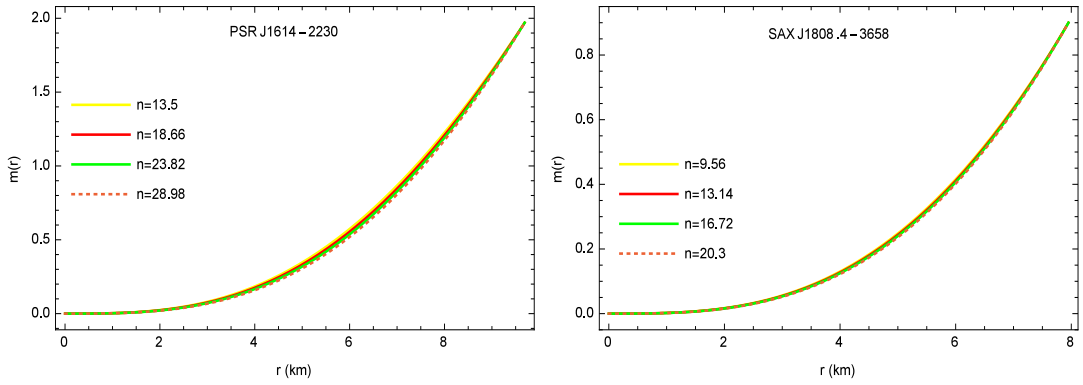

Fig. 6 Variation of mass ($m(r)$) with r for (i) PSR J1614–2230 with mass $M = 1.97\,M_\odot$ and radius $R = 9.69$ km for the models $n = 13.5,\ 18.66,\ 23.82$ and 28.98; (ii) SAX J1808.4–3658 with mass $M = 0.9\,M_\odot$ and radius $R = 7.951$ km for the models $n = 9.56,\ 13.14,\ 16.72$ and 20.3, and the values $b = 0.0001\,\mathrm{km}^{-2}$ and $c = 2.5$.

$\sqrt{-\frac{1}{g_{rr}}}\delta^j_r$ along r provide $g_{jk}v^jv^k = 1$ and $g_{jk}\chi^j\chi^k = -1$ respectively.

The line element (1) and momentum tensor T_{jk} (2) give rise to the following system of equations (Maurya et al. 2019c)

$$8\pi\rho = \frac{\left(1-e^{-\lambda(r)}\right)}{r^2} + \frac{\lambda'(r)e^{-\lambda(r)}}{r}, \tag{3}$$

$$8\pi p_r = \frac{\nu'(r)e^{-\lambda(r)}}{r} - \frac{\left(1-e^{-\lambda(r)}\right)}{r^2}, \tag{4}$$

$$8\pi p_t = \frac{e^{-\lambda}}{4}\left(2\nu'' + \nu'^2 - \nu'\lambda' + \frac{2\nu'}{r} - \frac{2\lambda'}{r}\right), \quad (5)$$

where $(')$ signifies derivative with respect to the radial coordinate r.

Considering the field equations, Equations (4) and (5), the anisotropic factor (Δ) takes the form

$$\begin{aligned}\Delta &= p_t - p_r \\ &= e^{-\lambda}\left[\frac{\nu''}{2} - \frac{\lambda'\nu'}{4} + \frac{\nu'^2}{4} - \frac{\nu'+\lambda'}{2r} + \frac{e^{\lambda}-1}{r^2}\right].\end{aligned} \quad (6)$$

Here we choose the gravitational constant G and speed of sound c to be unity.

3 THE KARMARKAR CONDITION

The Karmarkar condition required for the spacetime to be type class I embedding is

$$R_{1414} = \frac{R_{1212}R_{3434} + R_{1224}R_{1334}}{R_{2323}}, \quad (7)$$

subject to $R_{2323} \neq 0$ (Pandey & Sharma 1981).

The non-zero Riemann tensor components for the line element (1) are

$$R_{1414} = -e^{\nu(r)}\left(\frac{\nu''(r)}{2} + \frac{\nu'^2(r)}{4} - \frac{\lambda'(r)\nu'(r)}{4}\right), \quad (8)$$

$$R_{2323} = -e^{-\lambda(r)}r^2\sin^2\theta(e^{\lambda(r)} - 1), \quad (9)$$

$$R_{1212} = \frac{1}{2}r\lambda'(r), \quad (10)$$

$$R_{3434} = -\frac{1}{2}r\sin^2\theta\nu'(r)e^{\nu(r)-\lambda(r)}. \quad (11)$$

The differential equation derived using the Karmarkar condition (7) assumes the form

$$\frac{2\nu''}{\nu'} + \nu' = \frac{\lambda' e^{\lambda(r)}}{e^{\lambda(r)} - 1}. \quad (12)$$

Solving Equation (12), we find the following relation between $e^{\lambda(r)}$ and $e^{\nu(r)}$

$$e^{\lambda(r)} = \left(P + Q\int_0^r \sqrt{e^{\lambda(r)} - 1}dr\right)^2, \quad (13)$$

where P and Q are integration constants.

In view of Equation (6), the anisotropy of the fluid Δ (Maurya et al. 2016) is obtained as

$$\Delta = \frac{\nu'(r)}{4e^{\lambda(r)}}\left[\frac{2}{r} - \frac{\lambda'(r)}{e^{\lambda(r)}-1}\right]\left[\frac{\nu'(r)e^{\nu(r)}}{2rB^2} - 1\right]. \quad (14)$$

At this juncture, we should point out that when $\Delta = 0$, the only bounded solution simultaneously satisfying the Karmarkar condition and pressure isotropy is the interior Schwarzschild solution. This solution suffers various shortcomings including superluminal speeds within the interior of the fluid. To this end, we consider a solution describing an anisotropic fluid distribution which will be taken up in the next section.

4 A NEW PARAMETRIC CLASS OF SOLUTIONS

In this paper, we assumed the following metric potential

$$e^{\lambda(r)} = 1 + ar^2\alpha_n(r), \quad (15)$$

where

$$\alpha_n(r) = \csc^n\left(br^2 + c\right),$$

and a, b and c are positive constants and $n \geq 0$. We have selected $e^{\lambda(r)}$ such that at the center $e^{\lambda(r)} = 1$, which emphasises that at the center the tangent 3-space is flat and the EFEs can be integrated. Substituting $e^{\lambda(r)}$ from Equation (15) into Equation (13), we obtain the remaining metric potential $e^{\nu(r)}$ as

$$e^{\nu(r)} = \left(P - \frac{Qh_1(r)h_2(r)\sqrt{a\alpha_n(r)}}{4b}\right)^2, \quad (16)$$

where P and Q are integration constants.

Relying on the metric potentials given by Equations (15) and (16), the expressions for ρ, p_r, Δ and p_t can be cast as

$$\rho = \frac{a\alpha_n(r)\left(r^2\left(a\alpha_n(r) - 2bn\cot\left(br^2+c\right)\right) + 3\right)}{\left(ar^2\alpha_n(r)+1\right)^2}, \quad (17)$$

$$p_r = \frac{h_2(r)\sqrt{a\alpha_n(r)}}{h_3(r)\left(ar^2\alpha_n(r)+1\right)}, \quad (18)$$

$$\Delta = \frac{h_5(r)r^2\left(2bh_6(r) - h_7(r)\right)}{h_8(r)\left(1 + ar^2\alpha_n(r)\right)^2}, \quad (19)$$

$$p_t = p_r + \Delta, \quad (20)$$

where

$$\begin{aligned}h_1(r) &= {}_2F_1\left(\frac{1}{2}, \frac{n+2}{4}; \frac{3}{2}; \cos^2\left(br^2+c\right)\right), \\ h_2(r) &= \sin\left(2\left(br^2+c\right)\right)\sin^2\left(br^2+c\right)^{\frac{n-2}{4}}, \\ h_3(r) &= 2Pb\sqrt{a\alpha_n} - aQh_1(r)\sqrt{\alpha_n}\cos\left(br^2+c\right) \\ &\quad -4bQ, \\ h_4(r) &= \sqrt{a}Qh_1(r)\cos\left(br^2+c\right) - 2Pb, \\ h_5(r) &= a\alpha_n(r) + bn\cot\left(br^2+c\right), \\ h_6(r) &= aP\alpha_n(r) - Q\sqrt{a\alpha_n(r)}, \\ h_7(r) &= aBh_4(r)\cos\left(br^2+c\right)\csc^{\frac{n}{2}}\left(br^2+c\right), \\ h_8(r) &= 2Pb - \sqrt{a}Qh_1(r)\cos\left(br^2+c\right).\end{aligned}$$

The mass function $m(r)$, gravitational redshift $z(r)$ and compactification factor $u(r)$ at the surface and within the interior of the stellar system are expressed as

$$m(r) = \frac{ar^3\alpha_n(r)}{2\left(ar^2\alpha_n(r)+1\right)}, \quad (21)$$

$$z(r) = \frac{1}{P - \frac{Qh_1(r)h_2(r)\sqrt{a\alpha_n(r)}}{4b}} - 1, \quad (22)$$

$$u(r) = \frac{m(r)}{r} = \frac{ar^2\alpha_n(r)}{2\left(ar^2\alpha_n(r)+1\right)}. \quad (23)$$

5 MATCHING OF INTERIOR AND EXTERIOR SPACETIME OVER THE BOUNDARY

To determine the constants $a,\ b,\ c,\ P$ and Q appearing in our class of solutions, the interior metric must be matched smoothly across the boundary with the exterior Schwarzschild solution

$$ds^2 = \left(1-\frac{2M}{r}\right)dt^2 - \left(1-\frac{2M}{r}\right)^{-1}dr^2 - r^2(d\theta^2+\sin^2\theta d\phi^2)\,. \tag{24}$$

By comparing the interior solution (1) with exterior solution (24) at the boundary $r = R$ (Darmois-Isreal conditions), we obtain

$$e^{\nu_b} = 1-\frac{2M}{R} = \left(P+\frac{Q\left(n\sqrt{1-\gamma}+2bR^2+2c\right)\sqrt{a\alpha_n(R)}}{b\left(n^2+4\right)}\right)^2, \tag{25}$$

$$e^{-\lambda(r)_b} = 1-\frac{2M}{R} = \frac{1}{1+aR^2\alpha_n(R)}, \tag{26}$$

$$p_r(R) = 0. \tag{27}$$

With the help of the boundary conditions (25)–(27), we obtain

$$a = -\frac{2M\csc^{-n}\left(bR^2+c\right)}{R^2(2M-R)}, \tag{28}$$

$$P = \frac{\sqrt{1-\frac{2M}{R}}\left(ah_1(R)\cos\left(bR^2+c\right)\sqrt{\alpha_n(R)}+4b\right)}{4b}, \tag{29}$$

$$Q = \frac{1}{2}\sqrt{1-\frac{2M}{R}}\sqrt{a\csc^n\left(bR^2+c\right)}, \tag{30}$$

where $\gamma = \left(bR^2+c\right)^2$.

The constants b and c are free parameters and are selected in such a way that all the physical properties of the assumed stars for a suitable range of n are well-behaved and satisfy the Darmois-Israel conditions. The values of P and Q are expressed in Equations (29) and (30) respectively.

6 DISCUSSION OF PHYSICAL FEATURES FOR WELL-BEHAVED SOLUTIONS

6.1 Geometrical Regularity

The metric potentials (geometrical parameters) for the stars PSR J1614–2230 and SAX J1808.4–3658 for the range of n mentioned in Table 1 at the center $(r = 0)$ give the values $e^{\nu}|_{r=0}$ = positive constant and $e^{-\lambda(r)}|_{r=0} = 1$. This affirms that the metric potentials are regular and free from geometric singularities inside the stars. Also, both metric potentials $e^{\nu}(r)$ and $e^{-\lambda(r)}$ are monotonically increasing and decreasing respectively, with r (Fig.1).

6.2 Viable Trends in Physical Parameters

6.2.1 Density and pressure trends

The matter density ρ, radial pressure p_r and transverse pressure p_t for stars PSR J1614–2230 and SAX J1808.4–3658 are non-negative inside the stars and monotonically decrease from the center to the surface of these stars for the range of n mentioned in Table 1 (Figs. 2 and 3) (Zeldovich & Novikov 1971; Ivano 2002).

6.2.2 Relation between pressure-density ratios (Equation of state)

We plot the graphs of the EoS parameters $(p_r/\rho,\ p_t/\rho)$ to establish some connection between density and pressures. Using the trend of plots, we establish a linear, quadratic or Courant Friedrichs Lewy (CFL) EoS for our model. An example of starting off with the metric functions and then establishing an EoS is the classic paper by Mukherjee et al. (1997). In this work, they demonstrate that the Vaidya-Tikekar geometry leads to a linear EoS. From the plots of figures, we observe the decreasing trend of pressure to density ratios with r (Fig. 4) for both the stars PSR J1614–2230 and SAX J1808.4–3658 for the range of n mentioned in Table 1. Based on the trends in the plots, we calculate EOS for neutron star PSR J1614–2230 as

$$p_r = 0.861538\rho^2 + 0.206369\rho - 0.00223306, \tag{31}$$

$$p_r = 69.1848\rho^2 - 1.27803\rho + 0.00560289, \tag{32}$$

for $n = 13.5$ and $n = 28.98$ respectively and for the strange star SAX J1808.4-3658 as

$$p_r = 0.276979\rho^2 + 0.155325\rho - 0.00151322, \tag{33}$$

$$p_r = 48.6746\rho^2 - 0.639035\rho + 0.00149093, \tag{34}$$

for $n = 9.56$ and $n = 20.3$ respectively, following the method of least squares (elaborated on in the Appendix). The profiles of EoS for PSR J1614–2230 ($n = 13.5$) and SAX J1808.4–3658 ($n = 9.56$) are exhibited in Figure 5. The trends of EOS for other values of n in their corresponding ranges of the stars remain the same as in Figure 5.

6.2.3 Mass-radius relation, redshift and compactification factor

The mass function $m(r)$ and gravitational redshift $z(r)$ function of stars PSR J1614–2230 and SAX J1808.4–3658

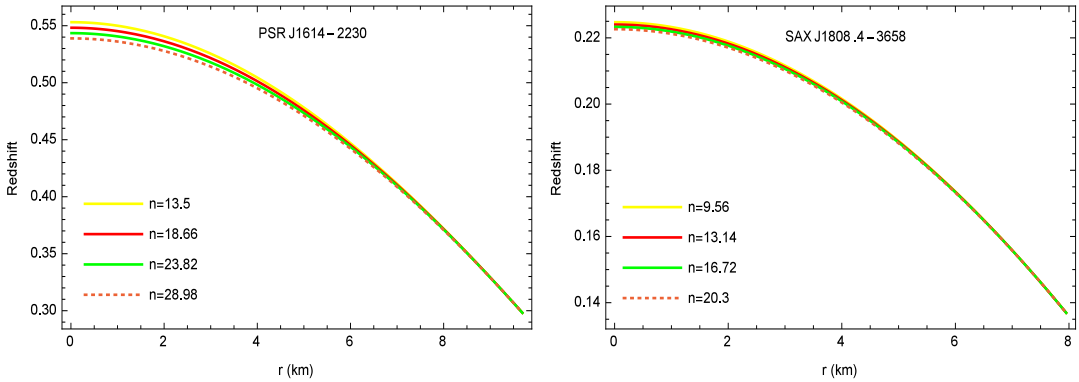

Fig. 7 Variation of redshift with r for (i) PSR J1614–2230 with mass $M = 1.97\,M_{\odot}$ and radius $R = 9.69$ km for the models $n = 13.5,\ 18.66,\ 23.82$ and 28.98; (ii) SAX J1808.4–3658 with mass $M = 0.9\,M_{\odot}$ and radius $R = 7.951$ km for the models $n = 9.56,\ 13.14,\ 16.72$ and 20.3, and the values $b = 0.0001\,\text{km}^{-2}$ and $c = 2.5$.

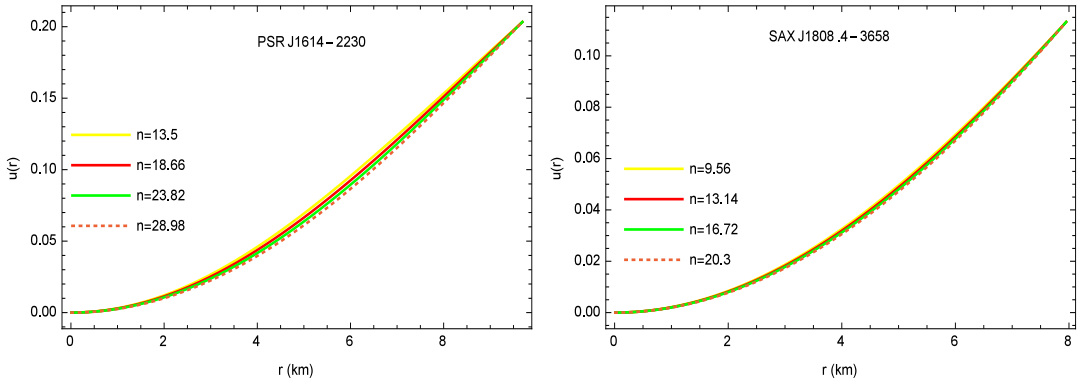

Fig. 8 Variation of the compactification factor $u(r)$ with r for (i) PSR J1614–2230 with mass $M = 1.97\,M_{\odot}$ and radius $R = 9.69$ km for the models $n = 13.5,\ 18.66,\ 23.82$ and 28.98; (ii) SAX J1808.4–3658 with mass $M = 0.9\,M_{\odot}$ and radius $R = 7.951$ km for the models $n = 9.56,\ 13.14,\ 16.72$ and 20.3, and the values $b = 0.0001\,\text{km}^{-2}$ and $c = 2.5$.

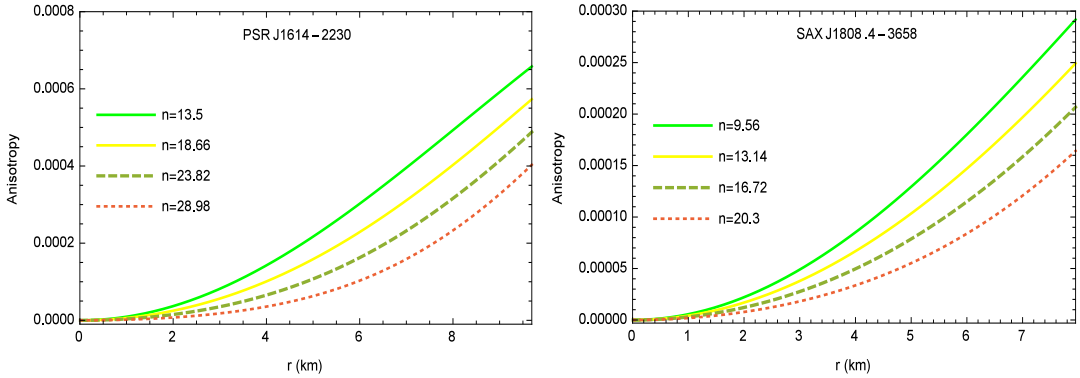

Fig. 9 Variation of anistropy $\Delta(r)$ with r for (i) PSR J1614–2230 with mass $M = 1.97\,M_{\odot}$ and radius $R = 9.69$ km for the models $n = 13.5,\ 18.66,\ 23.82$ and 28.98; (ii) SAX J1808.4–3658 with mass $M = 0.9\,M_{\odot}$ and radius $R = 7.951$ km for the models $n = 9.56,\ 13.14,\ 16.72$ and 20.3, and the values $b = 0.0001\,\text{km}^{-2}$ and $c = 2.5$.

for the range of n mentioned in Table 1 are increasing and decreasing respectively with r. The variation of $m(r)$ and $z(r)$ is plotted in Figures 6 and 7. Also, values of compactification parameter $u(r)$ for both the stars are increasing functions with r, displayed in Figure 8 and lying within the Buchdahl limit (Buchdahl 1959).

6.2.4 Anisotropic parameter

In Figure 9, the radial pressures (p_r) coincide with tangential pressure (p_t) at the centers of stars PSR J1614–2230 and SAX J1808.4–3658 for the range of n mentioned in Table 1, i.e., pressure anisotropies vanish at the center,

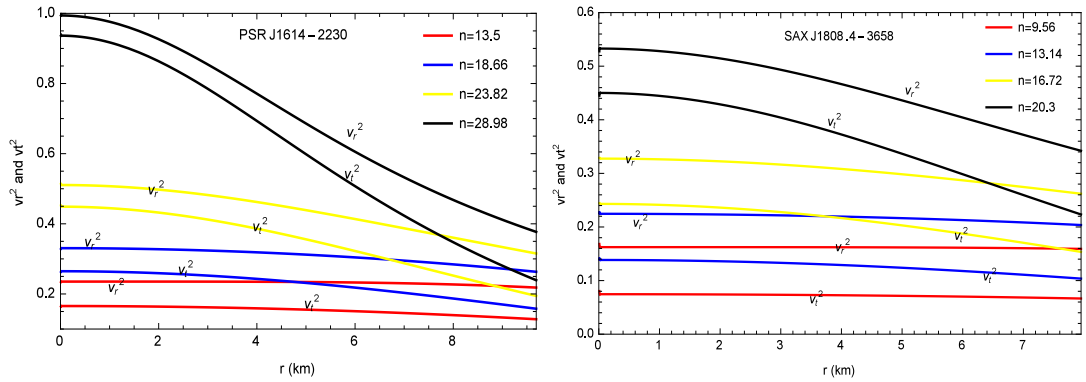

Fig. 10 Variation of v_r^2 and v_t^2 with r for (i) PSR J1614–2230 with mass $M = 1.97\,M_\odot$ and radius $R = 9.69$ km for the models $n = 13.5,\ 18.66,\ 23.82$ and 28.98; (ii) SAX J1808.4–3658 with mass $M = 0.9\,M_\odot$ and radius $R = 7.951$ km for the models $n = 9.56,\ 13.14,\ 16.72$ and 20.3, and the values $b = 0.0001\,\mathrm{km}^{-2}$ and $c = 2.5$.

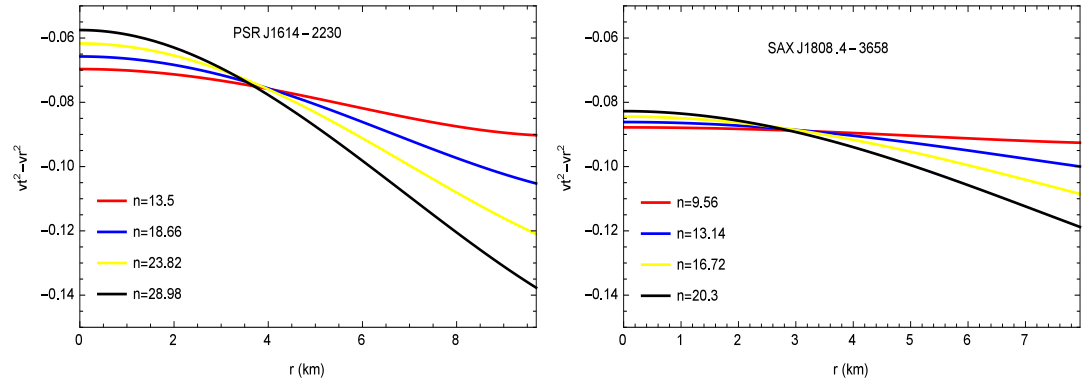

Fig. 11 Variation of ${v_t}^2 - {v_r}^2$ with r for (i) PSR J1614–2230 with mass $M = 1.97\,M_\odot$ and radius $R = 9.69$ km for the models $n = 13.5,\ 18.66,\ 23.82$ and 28.98; (ii) SAX J1808.4–3658 with mass $M = 0.9\,M_\odot$ and radius $R = 7.951$ km for the models $n = 9.56,\ 13.14,\ 16.72$ and 20.3, and the values $b = 0.0001\,\mathrm{km}^{-2}$ and $c = 2.5$.

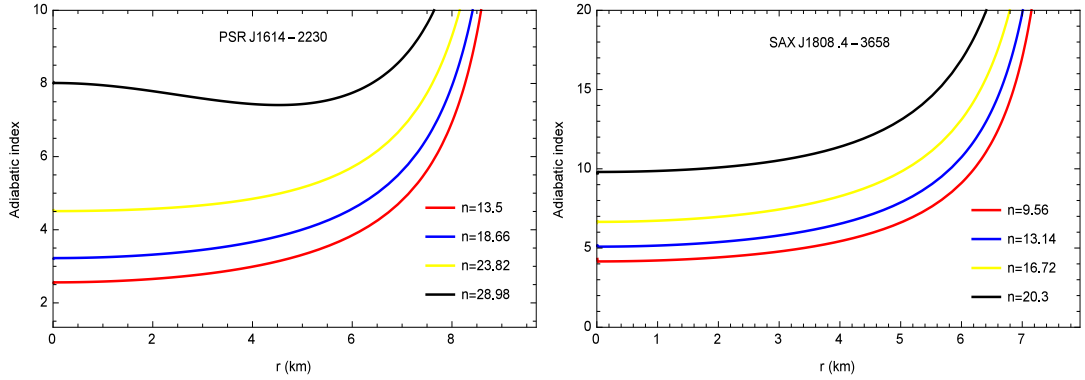

Fig. 12 Variation of $\Gamma(r)$ with r for (i) PSR J1614–2230 with mass $M = 1.97\,M_\odot$ and radius $R = 9.69$ km for the models $n = 13.5,\ 18.66,\ 23.82$ and 28.98; (ii) SAX J1808.4–3658 with mass $M = 0.9\,M_\odot$ and radius $R = 7.951$ km for the models $n = 9.56,\ 13.14,\ 16.72$ and 20.3, and the values $b = 0.0001\,\mathrm{km}^{-2}$ and $c = 2.5$.

$\Delta(0) = 0$ and increase outwards (Bowers & Liang 1974; Ivano 2002).

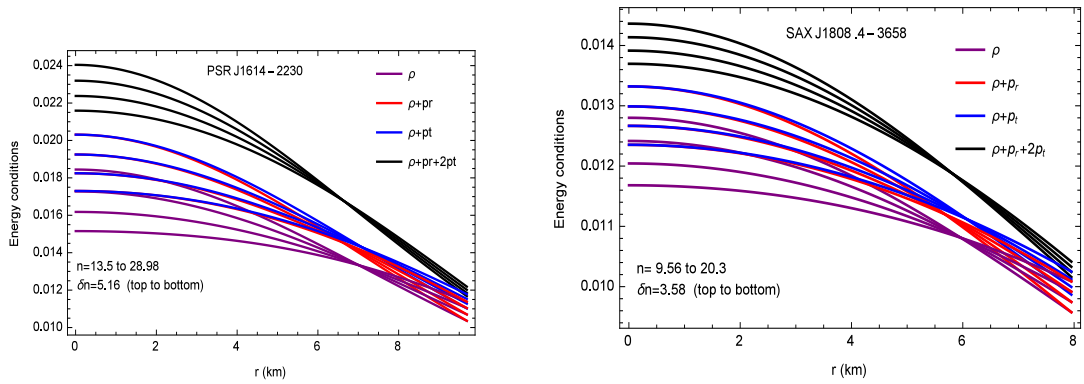

Fig. 13 Variation of energy conditions with r for (i) PSR J1614–2230 with mass $M = 1.97\,M_{\odot}$ and radius $R = 9.69$ km for the models $n = 13.5,\ 18.66,\ 23.82$ and 28.98; (ii) SAX J1808.4–3658 with mass $M = 0.9\,M_{\odot}$ and radius $R = 7.951$ km for the models $n = 9.56,\ 13.14,\ 16.72$ and 20.3, and the values $b = 0.0001\,\mathrm{km}^{-2}$ and $c = 2.5$.

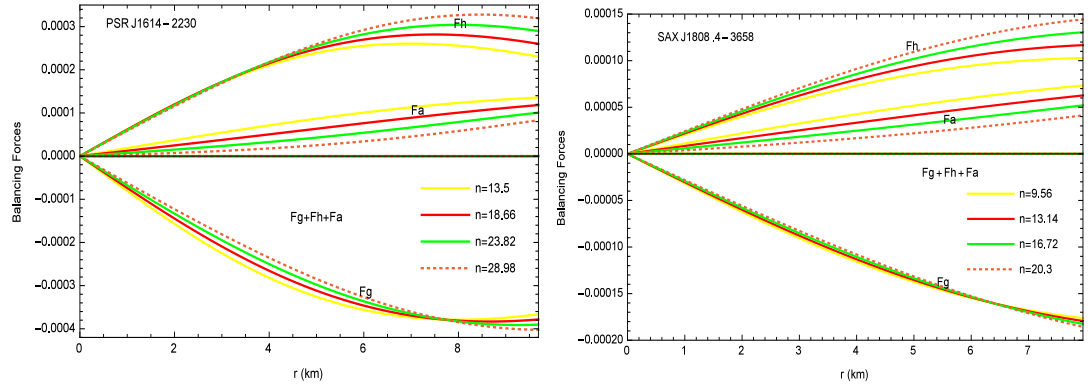

Fig. 14 Variation of balancing forces $F_a,\ F_g,\ F_a$ and $F_a + F_g + F_h$ with r for (i) PSR J1614–2230 with mass $M = 1.97\,M_{\odot}$ and radius $R = 9.69$ km for the models $n = 13.5,\ 18.66,\ 23.82$ and 28.98; (ii) SAX J1808.4-3658 with mass $M = 0.9\,M_{\odot}$ and radius $R = 7.951$ km for the models $n = 9.56,\ 13.14,\ 16.72$ and 20.3, and the values $b = 0.0001\,\mathrm{km}^{-2}$ and $c = 2.5$.

7 PHYSICAL STABILITY ANALYSIS

7.1 Zeldovich's Condition

The values of p_r, p_t and ρ at the center are given by

$$8\pi p_{rc} = 8\pi p_{tc} = a\csc^n(c)\frac{\left(-2Pb\sqrt{a\csc^n(c)} + 4bQ + \beta_1\beta_2 Q\right)}{\left(2Pb\sqrt{a\csc^n(c)} - \beta_1\beta_2 Q\right)} > 0, \tag{35}$$

and

$$8\pi\rho_c = 3a\csc^n(c) > 0 \ \ if \ \ a > 0\,. \tag{36}$$

Using Zeldovich's condition (Zeldovich & Novikov 1971), i.e., $p_{rc}/\rho_c \leq 1$, we get

$$\frac{-2Pb\sqrt{a\csc^n(c)} + 4bQ + \beta_1\beta_2 Q}{3\left(2Pb\sqrt{a\csc^n(c)} - \beta_1\beta_2 Q\right)} \leq 1. \tag{37}$$

In view of Equations (36) and (37), we get the following inequality

$$\frac{2Ab\sqrt{a\csc^n(c)}}{4b + \beta_1\beta_2} \leq \frac{Q}{P} \leq \frac{2Ab\sqrt{a\csc^n(c)}}{b + \beta_1\beta_2}, \tag{38}$$

where

$$\beta_1 = {}_2F_1\left(\frac{1}{2}, \frac{n+2}{4}; \frac{3}{2}; \cos^2(c)\right),$$
$$\beta_2 = a\cos(c)\sin^{\frac{n}{2}}(c)\csc^n(c).$$

7.1.1 *Hererra cracking stability of an anisotropic fluid sphere*

The Hererra cracking method (Herrera 1992) is used to analyse the stability of anisotropic stars under radial perturbations. We also employ the concept of cracking due to Abreu et al. (2007) to analyse potentially stable regions within the stellar configuration by subjecting our model to the condition $-1 < v_t^2 - v_r^2 \leq 0$

$$\frac{dp_t}{d\rho} = \frac{dp_r}{d\rho} + \frac{d\Delta}{d\rho} = \frac{dp_r}{d\rho} + \frac{d\Delta}{d\rho}\frac{dr}{d\rho}, \tag{39}$$

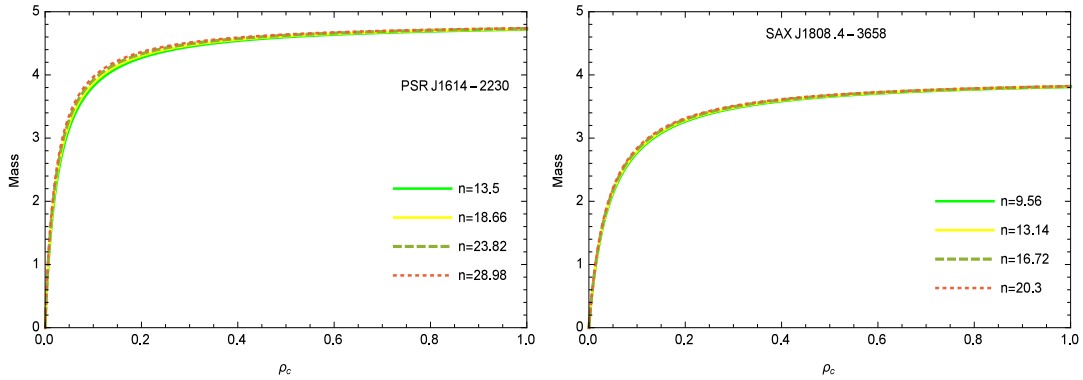

Fig. 15 Variation of mass with central density ρ_c for (i) PSR J1614–2230 with mass $M = 1.97\,M_\odot$ and radius $R = 9.69$ km for the models $n = 13.5,\ 18.66,\ 23.82$ and 28.98; (ii) SAX J1808.4–3658 with mass $M = 0.9\,M_\odot$ and radius $R = 7.951$ km for the models $n = 9.56,\ 13.14,\ 16.72$ and 20.3, and the values $b = 0.0001\,\text{km}^{-2}$ and $c = 2.5$.

$$v_r^2 - v_t^2 = -\frac{d\Delta}{d\rho}\frac{dr}{d\rho}. \tag{40}$$

For a physically feasible model of an anisotropic fluid sphere, the radial and transverse velocities of sound should be less than 1, which are referred to as causality conditions in the literature. The profiles of v_r^2 and v_t^2 of stars PSR J1614–2230 and SAX J1808.4–3658 for the range of n mentioned in Table 1 are given in Figure 10, which shows that $0 < v_r^2 \leq 1$ and $0 < v_t^2 \leq 1$ everywhere within the stellar configuration. Therefore, both the speeds satisfy the causality conditions and monotonically decreasing nature. Here, we follow the Herrera cracking method (Herrera 1992) for analysing the stability of anisotropic stars under radial perturbations. Using the concept of cracking, Abreu et al. (2007) put forth the idea that the region of an anisotropic fluid sphere where $-1 < v_t^2 - v_r^2 \leq 0$ is potentially stable. Figure 11 clearly depicts that our model is potentially stable inside both the stars PSR J1614–2230 and SAX J1808.4–3658 for the range of n mentioned in Table 1.

7.1.2 *Bondi stability condition for adiabatic index*

For a relativistic anisotropic sphere, the stability depends on the adiabatic index Γ_r and the ratio of two specific heats, defined by Heintzmann & Hillebrandt (1975),

$$\Gamma_r = \frac{\rho + p_r}{p_r}\frac{\partial p_r}{\partial \rho}.$$

Bondi (1964) suggested that for a stable Newtonian sphere, the Γ value should be greater than $\frac{4}{3}$. For an anisotropic relativistic sphere the stability condition is reported by Chan et al. (1993),

$$\Gamma > \tfrac{4}{3} + \Big[\tfrac{4(p_{t0}-p_{r0})}{3|p'_{r0}|r} + \tfrac{\rho_0 p_{r0}}{2|p'_{r0}|}r\Big],$$

where p_{r0}, p_{t0} and ρ_0 represent the initial radial pressure, tangential pressure and energy density respectively in static equilibrium. The first and last terms inside the square brackets represent the anisotropic and relativistic corrections respectively. Moreover, both these quantities are positive and increase the unstable range of Γ.

Chandrasekhar (1964a) established a condition on Γ to study the stability of the interior of the Schwarzschild metric and it is defined as

$$\Gamma > \Gamma_{cr} = \frac{4}{3} + \frac{19}{42}(2\delta), \tag{41}$$

where δ is compactification factor and Γ_{cr} is the critical adiabatic index which is determined from neutral configuration.

Moustakidis (2017) suggested that in the interior of a fluid sphere, Γ_{cr} should linearly depend on the pressure and density ratios at the center and $\Gamma > \Gamma_{cr}$. For a stable Newtonian sphere, Bondi and Chandrasekhar suggested that $\Gamma > \frac{4}{3}$ (Bondi 1964; Chandrasekhar 1964a,b).

The present class of models satisfies Bondi, Chandrasekhar and Moustakidis conditions for both compact stars PSR J1614-2230 and SAX J1808.4–3658 for the range of n mentioned in Table 1 and Γ_{cr} linearly depends on the ratio $\frac{p_r(0)}{\rho(0)}$.

7.1.3 *Energy conditions*

For a physically stable static model, the interior of the star should satisfy (i) null energy condition $\rho + p_r \geq 0$ (NEC) (ii) weak energy conditions $\rho + p_r \geq 0$, $\rho \geq 0$ (WEC$_r$) and $\rho + p_t \geq 0$, $\rho \geq 0$ (WEC$_t$) and (iii) strong energy condition $\rho + p_r + 2p_t \geq 0$ (SEC) (Maurya et al. 2019b). The profiles of energy conditions, i.e. NEC, WEC and SEC, are displayed in Figure 13 and our models satisfy all the energy conditions for both the stars PSR J1614–2230 and SAX J1808.4–3658 for the range of n mentioned in Table 1.

7.2 Tolman-Oppenheimer-Volkoff Condition for Equilibrium Under Three Forces

The Tolman-Oppenheimer-Volkoff (TOV) equation (Ponce de Leon 1987) for an anisotropic fluid matter distribution is expressed as

$$-\frac{M_g(r)(\rho+p_r)}{r^2}\,e^{(\lambda(r)-\nu(r))/2}-\frac{dp_r}{dr}+\frac{2\Delta(r)}{r}=0, \tag{42}$$

where F_g, F_h and F_a are gravitational, hydrostatic and anisotropic forces respectively and $M_g(r)$ is the gravitational mass that can be obtained from the Tolman-Whittaker formula

$$M_g(r) = \frac{1}{2}\,r^2\nu'(r)e^{(\nu(r)-\lambda(r))/2}. \tag{43}$$

The TOV equation, Equation (42), can be expressed in the following balanced force equation

$$F_g + F_h + F_a = 0. \tag{44}$$

In an equilibrium state, the three forces F_g, F_h and F_a satisfy the TOV equation. The profiles of the three forces of the stars PSR J1614–2230 and SAX J1808.4–3658 are exhibited in Figure 14 in which F_g overshadows the other two forces F_h and F_a such that the system is in static equilibrium.

7.3 Harrison-Zeldovich-Novikov Static Stability Criterion

The Harrison-Zeldovich-Novikov static stability criteria for non-rotating spherically symmetric equilibrium stellar models assert that the mass of compact stars must be an increasing function of its central density under small radial pulsation, i.e.,

$$\frac{\partial M}{\partial \rho_c} > 0\,. \tag{45}$$

This criterion ensures that the model is static and stable. It was proposed by Harrison et al. (1965) and Zeldovich & Novikov (1971) independently for stable stellar models. With the help of Equation (36) and total mass

$$M = m(R) = \frac{aR^3\csc^n\left(bR^2+c\right)}{2\left(aR^2\csc^n\left(bR^2+c\right)+1\right)}. \tag{46}$$

The expression of mass in terms of the central density is given by

$$M(\rho_c) = \frac{\rho R^3\csc^{-n}(c)\csc^n\left(bR^2+c\right)}{2\left(\rho R^2\csc^{-n}(c)\csc^n\left(bR^2+c\right)+3\right)}.$$

Also,

$$\frac{\partial M}{\partial \rho_c} = \frac{R^3\csc^{-n}(c)\csc^n\left(bR^2+c\right)}{6\left(\frac{1}{3}\rho R^2\csc^{-n}(c)\csc^n\left(bR^2+c\right)+1\right)^2} > 0$$

satisfies (Fig. 15) the static stability criterion (45).

The Harrison-Zeldovich-Novikov condition is satisfied for both the stars PSR J1614–2230 and SAX J1808.4–3658 for the range of n mentioned in Table 1.

8 DISCUSSION AND CONCLUSION

Our aim in this paper is to use the Karmarkar condition (which is purely geometric) to establish a physically viable stellar model (albeit a toy model). Toy models are important as they give a sense of the behaviour of the various physical and thermodynamical properties of the star and assist in setting up numerical codes and simulations.

In this paper, we have explored a new parametric class of solutions for anisotropic matter distribution to model the compact star PSR J1614–2230 and strange star SAX J1808.4–3658 by invoking the Karmarkar condition and adopting a form for one of the metric potentials, $e^{\lambda(r)}$. We find a range for one of the parameters, n for both stars such that the solutions are well behaved for particular choices of the free constants b and c. We have analysed all the geometrical and physical properties of these two stars and verified the physical viability of the solutions for the same range of n.

The graphs of the two stars for different models, i.e., (i) $n = 13.5,\ 18.66,\ 23.82$ and 28.98 for PSR J1614–2230; (ii) $n = 9.56,\ 13.14,\ 16.72$ and 20.3 for SAX J1808.4–3658 for parameter values of $b = 0.0001\,\mathrm{km}^{-2}$ and $c = 2.5\,\mathrm{km}^{-2}$, are plotted to find the range of n such that the solutions are well behaved. Furthermore, we ascertained that the range of well behaved solutions for PSR J1614–2230 is $n = 13.5$ to 28.98 and for SAX J1808.4–3658 is $n = 9.56$ to 20.3, corresponding to the same parameter values b and c.

For any value in the range of n, the geometrical parameters ($e^{-\lambda(r)}$ and $e^{\nu(r)}$) are decreasing and increasing respectively throughout the interior of the stars and both curves meet at their boundary (Fig. 1). For physical parameters such as density, radial and tangential pressures, pressure to density ratios and redshift, both the velocities in that range of n are non-negative at the center and monotonically decrease from the center to surface of the stars (Figs. 2, 3, 4, 7 and 10). Physical parameters mass, compactification factor, anisotropy and adiabatic index are increasing outward, which is required for a physically viable stellar configuration (Figs. 6, 8, 9 and 12).

Our models satisfy all the stability conditions for the two stars for any value of n in that range, i.e., Herrera cracking condition ($-1 < v_t^2 - v_r^2 < 0$, $0 < v_r^2,\ v_t^2 < 1$), Bondi condition ($\Gamma > 4/3$), Zeldovich's condition ($0 < \frac{p_r}{\rho},\ \frac{p_r}{\rho} < 1$) and Harrison-Zeldovich-Novikov criterion ($\frac{\partial M}{\partial \rho_c} > 0$) (Figs. 11, 12, 15). For the same range

Table 1 The variation in physical parameters, i.e., central adiabatic index, central density, central redshift, surface redshift and compactness factor, for different models of (i) PSR J1614–2230 with mass $M = 1.97\,M_\odot$ and radius $R = 9.69\,\mathrm{km}$ for parameters $n = 13.5,\ 18.66,\ 23.82$ and 28.98; (ii) SAX J1808.4–3658 with mass $M = 0.9\,M_\odot$ and radius $R = 7.951\,\mathrm{km}$ for parameters $n = 9.56,\ 13.14,\ 16.72$ and 20.3 for the values of $b = 0.0001\,\mathrm{km}^{-2}$, $c = 2.5$, $G = 6.67 \times 10^{-11}\,\mathrm{m}^3\,\mathrm{kg}^{-1}\,\mathrm{s}^{-2}$, $M_\odot = 2 \times 10^{30}\,\mathrm{kg}$ and $C = 3 \times 10^8\,\mathrm{m\,s}^{-1}$.

	$n = 13.5$	$n = 18.66$	$n = 23.82$	$n = 28.98$	$n = 9.56$	$n = 13.14$	$n = 16.72$	$n = 20.3$
Central adiabatic index (Γ_c)	2.5881	3.2254	4.5	8.0523	4.2634	5.1352	6.7296	9.76
Central density ($\rho_c\ g\,\mathrm{cm}^{-3} \times 10^{14}$)	4.8075	4.3597	3.9575	3.5959	3.6093	3.4397	3.2792	3.127
Central radial pressure (P_{r_c}) ($\mathrm{dyne\,cm}^{-2} \times 10^{34}$)	9.008	9.5265	9.9761	10.362	2.5136	2.7694	3.0125	3.2432
Central redshift (z_c)	0.5531	0.5482	0.5435	0.5389	0.22474	0.22402	0.22332	0.22262
Surface redshift (z_b)	0.29815	0.29815	0.29815	0.29815	0.13694	0.13694	0.13694	0.13694
Compactness factor $\frac{GM}{C^2R}$	0.30134	0.30134	0.30134	0.30134	0.16777	0.16777	0.16777	0.16777

of n for both stars, the present models hold for all the energy conditions ($\rho > 0$, $\rho + p_r > 0$, $\rho + p_t > 0$, $\rho + p_r + 2p_t > 0$) which are required for a physically viable configuration (Fig. 13). Furthermore, our models represent a static anisotropic stellar fluid in equilibrium configuration as the gravitational force, hydrostatic force and anisotropic force are, acting in the interiors of stars through the TOV equation, counterbalancing each other (Fig. 14).

The physical quantities, i.e., central adiabatic index (Γ_c), central density (ρ_c), central pressure (p_{r_c}), central redshift ($z_c(r)$), surface redshift ($z_s(c)$) and compactness factor ($u(r) = \frac{GM}{cR^2}$), are listed in Table 1. From Table 1 we conclude that with larger values of n, the central adiabatic index and central pressure are increasing, whereas the central density and central redshift are decreasing with increasing value of n. Other physical parameters, i.e., compactification factor and redshift at the surface, remain constant for any value in the range of n. This work has provided a family of parametric solutions of the EFEs obeying the Karmarkar condition. We show that these solutions are sufficiently useful to model compact objects and predict their observed stellar characteristics within very good approximation.

APPENDIX: GENERATING FUNCTION

All the spherically symmetric solutions can be generated from the two generating functions given by Herrera et al. (2008). The two primitive generating functions $\eta(r)$ and $\Pi(r)$ are defined as

$$e^{\nu(r)} = e^{\left[\int (2\eta(r) - \frac{2}{r})dr\right]},$$
$$\Pi(r) = 8\pi(p_r - p_t). \tag{47}$$

The two generating functions pertaining to the present class of solutions are obtained as

$$\eta(r) = \frac{\sqrt{a}Qh_1(r)\cos\left(br^2+c\right) - 2b\left(\sqrt{a}Qr^2\csc^{\frac{n}{2}}\left(br^2+c\right) + P\right)}{r\left(\sqrt{a}Qh_1(r)\cos\left(br^2+c\right) - 2Pb\right)}$$

and

$$\Pi(r) = 8\pi(p_r - p_t) = -8\pi\Delta\,.$$

APPENDIX: EQUATION OF STATE

The EoS is defined as the relation between radial pressure (p_r) and density (ρ) within a star. Since the transformation of p_r in terms of ρ is so cumbersome, here we exploit a curve fitting technique to approximate the EoS. Further, from Figure 10, we observe that the plot of $v_r = \sqrt{\frac{dp_r}{d\rho}}$ is not a straight line (i.e., $\frac{dp_r}{d\rho}$ is not a constant), therefore, it is necessary that the relation between p_r and ρ is parabolic in nature. Consequently, in order to get the EoS, we consider the curve fitting method for quadratic form

$$p_r(r) = U + T\rho(r) + S\rho^2(r), \tag{48}$$
$$\Sigma p_r(r) = 11U + T\Sigma\rho(r) + S\Sigma\rho^2(r), \tag{49}$$
$$\Sigma\rho(r)p_r(r) = U\Sigma\rho(r) + T\Sigma\rho^2(r) + S\Sigma\rho^3(r), \tag{50}$$
$$\Sigma\rho^2(r)p_r(r) = U\Sigma\rho^2(r) + T\Sigma\rho^3(r) + S\Sigma\rho^4(r), \tag{51}$$

where r varies from central to boundary of the star. To find the curve via the least squares method, we consider the points with differences 0.969 and 0.7951 for PSR J1614–2230 and SAX J1808.4–3658 respectively. Solving Equations (49), (50) and (51) for S, T and U and substituting the values in Equation (48), we arrive at the required EoS.

Acknowledgements The authors are thankful to the learned referee for valuable comments and suggestions that improved the paper.

References

Abreu, H., et al. 2007, Classical and Quantum Gravity, 24, 4631
Andreasson, H., Boehmer, C. G., & Mussa, A. 2012, Classical and Quantum Gravity, 29, 095012
Event Horizon Telescope Collaboration, Akiyama, K., et al. 2019, ApJL, 875, L1

Bejger, M., & Haensel, P. 2002, A&A, 396, 917
Bhar, P. 2019, Eur. Phys. J. C, 79, 138
Biswas, S., Shee, D., et al. 2019, Annals of Physics, 409, 167905
Bondi, H. 1964, Proc. R. Soc. Lond. A, 281, 39
Bowers, R. L., & Liang, E. P. T. 1974, ApJ, 188, 657
Buchdahl, H. A. 1959, Phys. Rev. D, 116, 1027
Chan, R., et al. 1993, MNRAS, 265, 533
Chan, R., Herrera, L., & Santos, N. O. 1994, MNRAS, 267, 637
Chandrasekhar, S. 1964, ApJ, 140, 417
Chandrasekhar, S. 1964, Phys. Rev. Lett., 12, 114
Dev, K., & Gleiser, M. 2002, Gen. Relativ. Gravit., 34, 1793
Dev, K., & Gleiser, M. 2003, Gen. Relativ. Gravit., 35, 1435
Di Prisco, A., Herrera, L., Le Denmat, G., et al. 2007, Phys. Rev. D, 76, 064017
Di Prisco, A., Herrera, L., Falcon, N., et al. 1997, Gen. Relativ. Gravit., 29, 1391
Fuloria, P. 2017, Astro. Phys. Space Sci., 362, 217
Gangopadhyay, T., et al. 2013, MNRAS, 431, 3216
Gedela, S., Bisht, R. K., & Pant, N. 2018, Eur. Phys. J. A, 54, 207
Gedela, S., Bisht, R. K., & Pant, N. 2019, Modern Physics Letters A, 34, 1950157
Gedela, S., Pant, R. P., Bisht, R. K., et al. 2019, Eur. Phys. J. A, 55, 95
Gedela, S., Pant, N., Pant, R. P., et al. 2019, Int. J. Mod. Phys. A., 34, 1950179
S. Gedela, Bisht, R. K., & Pant, N. 2020, Modern Physics Letters A, 35, 2050097
Ghosh, S. G., & Maharaj, S. D. 2015, Eur. Phys. J. C, 75, 7
Govender, G., Govender, M., & Govinder, K. S. 2010, Int. J. Mod. Phys. D, 19, 1773
Govender, M. 2013, Int. J. Mod. Phys. D, 22, 1350049
Govender, M., & Govinder, K. S. 2001, Phys. Lett. A, 283, 71
Guo, J., & Joshi, P. S. 2015, Phys. Rev. D, 92, 064013
Hansraj, S., & Mkhize, N. 2019, European Physical Journal Plus, 134, 137
Harrison, B. K., et al. 1965, Gravitational Theory and Gravitational Collapse, University of Chicago Press, Chicago
Heintzmann, H., & Hillebrandt, W. 1975, A&A, 38, 51
Herrera, L., & Martinez, J. 1998, Gen. Relativ. Gravit., 30, 445
Herrera, L. 1992, Phys. Lett. A, 165, 206
Herrera, L., Le Denmat, G., Marcilhacy, G., et al. 2005, Int. J. Mod. Phys. D, 14, 657
Herrera, L., et al. 2005, Gen. Relativ. Gravit., 37, 873
Herrera, L., Ospino, J., & Di Prisco, A. 2008, Phys. Rev. D, 77, 027502
Herrera, L., Le Denmat, G., & Santos, N. O. 1989, MNRAS, 237, 257
Ivanov, B. V. 2002, Phys. Rev. D, 65, 104011
Ivanov, B. V. 2018, Eur. Phys. J. C, 78, 332
Ivanov, B. V. 2020, Eur. Phys. J. Plus, 135, 377
Jasim, M. K., Maurya, S. K., & Al Sawaii, A. S. M. 2020, Astrophys Space Sci., 365, 9
Karmarkar, K. R. 1948, Proc. Indian. Acad. Sci. A, 27, 56, https://doi.org/10.1007/BF03173443
Karmarkar, S., Mukherjee, S., Sharma, R., et al. 2007, Pramana J. Phys., 68, 881
Manjonjo, A. M., Maharaj, S. D., & Moopanar, S. 2018, Classical and Quantum Gravity, 35, 045015
Maurya, S. K., & Govender, M. 2017, Eur. Phys. J. C, 77, 420
Maurya, S. K., et al. 2016, Eur. Phys. J. A 52, 191
Maurya, S. K., et al. 2019, Phys. Rev. D, 100, 044014
Maurya, S. K., et al. 2019, Phys. Rev. D, 99, 044029
Maurya, S. K., Maharaj, S. D., & Deb, D. 2019, Eur. Phys. J. C, 79, 170
Moustakidis, Ch. C. 2017, Gen. Relativ. Gravit., 49, 68
Mukherjee, S., Paul, B. C., & Dadhich, N. 1997, Class. Quantum Grav., 14, 3475
Naidu, N. F., Govender, M., & Maharaj, S. D. 2018, Eur. Phys. J. C, 78, 48
Oppenheimer, J. P., & Snyder, H. 1939, Phys. Rev., 56, 455
Pandey, S. N., & Sharma, S. P. 1981, Gen. Relativ. Gravit., 14, 113
Pant, N., Pradhan, N., & Bansal, R. K. 2016, Astrophys. Space Sci., 361, 41
Pant, N., Gedela, S., & Bisht, R. K. 2020, Chin. J. Phys. https://doi.org/10.1016/j.cjph.2020.06.020
Ponce de Leon, J. 1987, Gen. Relativ. Gravit. 19, 797
Santos, N. O. 1985, MNRAS, 216, 403
Sarkar, N., et al. 2020, Eur. Phys. J. C, 80, 255
Schwarzschild, K. 1916, Sitz. Deut. Akad.Wiss. Berlin Kl. Math. Phys., 1916, 189, arXiv:physics/9905030
Schwarzschild, K. 1916, Sitz. Deut. Akad.Wiss. Berlin Kl.Math. Phys., 24, 424. arXiv:physics/9912033.
Sharma, R., & Mukherjee, S. 2001, Mod. Phys. Lett. A, 16, 1049
Sharma, R., Mukherjee, S., & Maharaj, S. D. 2001, Gen. Relativ. Grav., 33, 999
Sharma, R., & Maharaj, S. D. 2007, A&A, 28, 133
Sherif, A., Goswami, R., & Maharaj, S. 2019, Classical and Quantum Gravity, 36, 215001
Singh, K. N., Pant, N., & Pradhan, N. 2016, Astrophys. Space Sci., 361, 173
Singh, K. N., et al. 2020, Chin. Phys. C, 44, 035101
Stephani, H., Kramer, D., et al. 2003, Exact Solutions of Einstein's Field Equations (2nd Edition, Cambridge Univ. Press)
Tello-Ortiz, F., Maurya, S. K., Errehymy, A., Singh, N. K., & Daoud, M. 2019, Eur. Phys. J. C, 79, 885
Upreti, J., Gedela, S., Pant, N., & Pant, R. P. 2020, New Astronomy, 80, 101403
Vaidya, P. C. 1951, Proc. Indian Acad. Sc. A, 33, 264
Zeldovich, Y. B., & Novikov, I. D. 1971, Relativistic Astrophysics, 1, Stars and Relativity, University of Chicago Press, Chicago